The shadow and observation appearance of black hole surrounded by the dust field in Rastall theory

Xuan-Ran Zhu(朱轩然)[1,†], Yun-Xian Chen(陈芸仙)[2,‡], Ping-Hui Mou(牟平辉)[2,§], and Ke-Jian He(何柯腱)[3,¶]

[1] *Chongqing College of Mobile Communication, Chongqing* 401520, *China*

[2] *Physics and Space College, China West Normal University, Nanchong* 637000, *China*

[3] *Department of Physics and Chongqing Key Laboratory for Strongly Coupled Physics, Chongqing University, Chongqing* 401331, *China*

(Received 4 March 2022; revised manuscript received 4 March 2022; accepted manuscript online 12 May 2022)

In the context of Rastall gravity, the shadow and observation intensity casted by the new Kiselev-like black hole with dust field have been numerically investigated. In this system, the Rastall parameter and surrounding dust field structure parameter have considerable consequences on the geometric structure of spacetime. Considering the photon trajectories near the black hole, we investigate the variation of the radii of photon sphere, event horizon and black hole shadow under the different related parameters. Furthermore, taking into account two different spherically symmetric accretion models as the only background light source, we also studied the observed luminosity and intensity of black holes. For the both spherical accretions background, the results show that the decrease or increase of the observed luminosity depends on the value range of relevant parameters, and the promotion effect is far less obvious than the attenuation effect on the observed intensity. One can find that the inner shadow region and outer bright region of the black hole wrapped by infalling accretion are significantly darker than those of the static model, which is closely related to the Doppler effect. In addition, the size of the shadow and the position of the photon sphere are always the same in the two accretion models, which means that the black hole shadow depend only on the geometry of spacetime, while the observation luminosity is affected by the form of accretion material and the related spacetime structure.

Keywords: Rastall gravity, black hole

PACS: 04.50.Kd, 04.70.–s, 04.40.Nr

DOI: 10.1088/1674-1056/ac6ee0

1. Introduction

One hundred years ago, Einstein proposed the general relativity describing the gravity successfully. The existence of black holes and gravitational waves, as the two most important predictions in general relativity, has always attracted close attention of scientists. In 2015, the gravitational wave event (GW150914) generated by the merger of two black holes was detected by the Laser Interferometer Gravitational Wave Observatory (LIGO).[1–3] It is not only provides the first direct evidence for the existence of black holes, but also encourages people to uncover the mysterious veil of black holes. As another important milestone in the history of black holes, the image of the supermassive black hole in M87* convincingly confirms that the black hole exists in our universe. This ultra-high angular resolution image comes from the international collaboration of Event Horizon Telescope (EHT).[4–7] From the image of the black hole, one can find that an asymmetric bright ring embedded in the dark background, in which, the bright ring is the photon ring, and the dark area inside the bright ring is called the shadow of black hole.

The strong gravity of black hole deflects light to form the shadow of the black hole, also known as the gravitational lensing effect. In 1966, Synge was the first to theoretically calculate the shadow of Schwarzschild black hole and the condition under which photons could escape to infinity was also given.[8] After that, the radius of photon ring for Schwarzschild black hole is $r = 5.2M$ (M is the mass of black hole) was proposed in Ref. [9]. While for a rotating spherically symmetric black hole, i.e., the Kerr black hole, the shape of shadow is decided by the rotating parameter, and the D-shape shadow can be obtained when the location of observer is fixed to the equatorial plane.[10,11] More research on black shadow can be seen in Refs. [12–40], the size and shape of the shadow for a rotating or non rotating black hole, and constraining black hole parameters with shadow have been studied in the general relativity and other modified gravitational backgrounds.

In our real universe, the black holes are surrounded by a large number of high energy radiative materials, which play an indispensable role in the observation of black hole shadow.[41] In 1979, the numerical simulation image of Schwarzschild black hole with the thin disk accretion was given by Luminet.[9] Taking into account the simplified model of accretion materials, that is, the black holes are obscured by the optically and thin spherically symmetric accretion,

†Corresponding author. E-mail: xuanranzhu@126.com

‡Corresponding author. E-mail: cyx17765580321@163.com

§Corresponding author. E-mail: mph2022@163.com

¶Corresponding author. E-mail: kjhe94@163.com

© 2023 Chinese Physical Society and IOP Publishing Ltd

Narayan *et al*. pointed out the size of the observed shadow depends on the spacetime geometry and is not affected by the surrounding accretion.[42] While in Ref. [43], the shadow of a black hole is related to the geometrically thick accretion disks. Moreover, it can be found that the observation intensity of black hole shadow is significantly different in static and infalling accretion models.[44,45] Using the optically and geometrically thin disk accretion model, Gralla *et al.* found that the rings outside the black hole shadow can be divided into direct rings, photon rings and lensing rings.[46] And, the position and observation intensity of these rings are both closely related to the relevant parameters of spacetime and the position of thin disk accretion. So far, some research results of black hole shadow surrounded by the different accretion models have been obtained.[47–63]

As described in the studies,[64,65] Rastall proposed a possible modification of the general theory of relativity in 1972. According to the Rastall gravity theory, the covariant derivative of the energy momentum tensor is no longer zero in curved spacetime, whereby avoids the problem that the covariant conservation relation of the energy–momentum tensor is only verified in the Minkowaski flat or weak field regime of gravity. Based on the background of Rastall theory, Heydarzade *et al.* obtained a new class of the Kiselev-like black hole solutions surrounded by perfect fluid, and they found that the corresponding effective complete fluid has different characteristics in different parameter ranges.[66] It means that Rastall parameter and surrounding field structure parameter can effectively describe the geometric structure of the spacetime. The physical characteristics of this class black hole models have also been studied, such as the thermodynamic behavior, quasinormal modes, and black hole shadow.[67–72] In Ref. [73], considering the black holes surrounded by perfect fluid radiation field in the Rastall theory, Guo *et al*. studied the shadow and observed luminosity of black hole. Nevertheless, the geometric effects of the Rastall parameters do not appear for the black hole surrounded by the radiation field.[66] In view of this, we focus primarily in this paper on the shadow and observed appearance of black hole surrounded by the dust field, where the Rastall geometric parameters exist. Due to the existence of Rastall geometric parameters, it can greatly change the causal structure of spacetime compared with the general theory of relativity. In particular, we want to study whether the change of the relevant parameters (the Rastall parameter and surrounding dust field structure parameter) will cause the change of shadow and photon sphere radius of black hole, or what kind of changes will be cause. In addition, we consider the emission form of the accretion material around the black hole is spherical symmetry, whereby to further study the influence of relevant parameters on the observed luminosity and appearance of black hole shadow, in these two accretion models.

The remainder of this paper is organized as follows. In Section 2, the black hole surrounded by the perfect fluid dust field in Rastall theory is briefly introduced, and the photon orbit and effective potential of the black hole are discussed. In Section 3, we show the shadow and photon sphere of the black hole in different spherical accretions, and the corresponding observed luminosity is also shown. We summarize results and discussions in the last section.

2. The black hole surrounded by dust field in Rastall theory and light deflection

Based on the hypothesis proposed by Rastall,[64,65] one can consider the Rastall field for a spacetime with Ricci scalar R and an energy momentum source $T_{\mu\nu}$, which leads to the modification of the Einstein's field equations as

$$G_{\mu\nu} = \kappa\left(T_{\mu\nu} - \lambda\,\delta_{\mu\nu}R\right), \tag{1}$$

where κ is the Rastall gravitational coupling constant and λ is the Rastall parameter, respectively. Note that the standard theory of general relativity can be traced back from Eq. (1) in the limit of $\lambda \to 0$. Then, the solution of a general spherical symmetric black hole surrounded by perfect fluid in Rastall theory could take the form[66]

$$\mathrm{d}s^2 = -N_{\mathrm{f}}(r)\,\mathrm{d}t^2 + \frac{\mathrm{d}r^2}{N_{\mathrm{f}}(r)} + r^2\,\mathrm{d}\Omega_{\mathrm{f}}^2, \tag{2}$$

with

$$\begin{aligned} N_{\mathrm{f}}(r) &= 1 - \frac{2M}{r} - \frac{N_{\mathrm{f}}}{r^{\sigma}}, \\ \sigma &= \frac{-6\kappa\lambda\left(\omega_{\mathrm{f}}+1\right)+3\omega_{\mathrm{f}}+1}{1-3\kappa\lambda\left(\omega_{\mathrm{f}}+1\right)}, \end{aligned} \tag{3}$$

in which $\mathrm{d}\Omega_{\mathrm{f}}^2 = \mathrm{d}\theta^2 + \sin^2(\theta)\,\mathrm{d}\varphi^2$. In the spacetime of Eq. (4), M is the mass of the black hole, and N_{f} is the intensity parameter of perfect fluid matter around black hole, respectively. For $\lambda \to 0$, it could recover the solution proposed by Kiselev in the framework of general relativity.[74] Then, we can get energy density $\rho_{\mathrm{f}}(r)$ of surrounding fluid[66] as

$$\rho_{\mathrm{f}}(r) = -\frac{3N_{\mathrm{f}}\mathcal{W}_{\mathrm{f}}}{\kappa r^{\frac{3(\omega_{\mathrm{f}}+1)-12\kappa\lambda(\omega_{\mathrm{f}}+1)}{1-3\kappa\lambda(\omega_{\mathrm{f}}+1)}}}, \tag{4}$$

where $\mathcal{W}_{\mathrm{f}}$ is a geometric constant depending on the Rastall geometric parameters κ and λ, as well as the state parameter of surrounding fluid ω_{f}, that is

$$\mathcal{W}_{\mathrm{f}} = \frac{\left(1-4\kappa\lambda\right)\left(\kappa\lambda\left(\omega_{\mathrm{f}}+1\right)-\omega_{\mathrm{f}}\right)}{\left(1-3\kappa\lambda\left(\omega_{\mathrm{f}}+1\right)\right)^2}. \tag{5}$$

To preserve the weak energy condition$\rho_f(r) \geq 0$, $\mathcal{W}_{\mathrm{f}}$ and N_{f} should follow the condition

$$N_{\mathrm{f}}\mathcal{W}_{\mathrm{f}} \leq 0. \tag{6}$$

Hence, the sign of parameter $N_{\rm f}$ is associated with each choice of the parameters $\kappa\lambda$. By considering the black hole surrounded by a dust field in Rastall gravity, i.e., $\omega_{\rm f}=0$, the metric function is given by[66,74,75]

$$N_{\rm d}(r)=1-\frac{2M}{r}-\frac{N_{\rm d}}{r^{\frac{1-6\kappa\lambda}{1-3\kappa\lambda}}}. \tag{7}$$

In Eq. (7), the Rastall correction term is not expressed as the mass term, which also brings new characteristics to the black hole due to the existence of Rastall parameters $\kappa\lambda$. Thus, the geometric parameters $\kappa\lambda$ of the Rastall theory can play an important role in leading to distinct solutions relative to general relativity. It is worth mentioning that the value of $N_{\rm d}$ follows the condition $0<N_{\rm d}$ for the case of $0\leq\kappa\lambda<1/4$, while for $\kappa\lambda<0\cup\kappa\lambda>1/4$ it needs $0>N_{\rm d}$. As we mentioned earlier, it is required that the weak energy condition represented by relation (6) is satisfied. Interestingly, there is an effective surrounding fluid accompanied by an effective equation of state parameters $\omega_{\rm eff}$ for the case $1/6<\kappa\lambda<1/3$, which explains the accelerating expansion of the universe in the Rastall theory of gravity, but the case violates the strong energy condition. In addition, the value of effective equation of state parameter $\omega_{\rm eff}$ may help to explain the deceleration expansion and even contraction of the universe when $\kappa\lambda$ values in the rang $1/6>\kappa\lambda$ or $1/3<\kappa\lambda$, which is conform to the strong energy condition.[66]

Since the wavelength of the actual light source is smaller than the size of the black hole, we can discuss the problem of black hole shadow in the scope of geometrical optics. That is, it is necessary to understand the motion behavior of photons in the spacetime near black holes. With the help of Euler–Lagrange equation, the motion equation of photon moving along geodesic can be expressed as

$$\frac{\rm d}{{\rm d}\xi}\left(\frac{\partial\mathcal{I}}{\partial\dot{x}^{\mu}}\right)=\frac{\partial\mathcal{I}}{\partial x^{\mu}}. \tag{8}$$

In the above equation, ξ is the affine parameter, $\dot{x}^{\mu}$ is the four-velocity of the light ray and $\mathcal{I}$ is Lagrangian, respectively. In addition, we also can get

$$\begin{aligned}\mathcal{I}&=\frac{1}{2}g_{\mu\nu}\dot{x}^{\mu}\dot{x}^{\nu}\\&=\frac{1}{2}\left[-N_{\rm d}(r)\dot{t}^2+\frac{\dot{r}^2}{N_{\rm d}(r)}+r^2\left(\dot{\theta}^2+\sin^2\theta\dot{\varphi}^2\right)\right].\end{aligned} \tag{9}$$

In the spherically symmetric space-time of Eq. (2), one can find that the metric coefficients do not depend explicitly on the time t and azimuthal angle φ. Hence, there are two conserved quantities, i.e., energy E and angular momentum L, which can be derived from the geodesic equations of the space-time Eq. (2). In addition, we are most interested in the light ray that moves on the equatorial plane, which means $\theta=\pi/2$ or $\dot{\theta}=0$.[56] Therefore, we can obtain

$$E=\dot{t}N_{\rm d}(r),\quad \dot{\varphi}=\pm\frac{1}{r^2}. \tag{10}$$

Substituting the above equations into Eq. (9), one can derive that

$$\dot{t}=\frac{1}{b_{\rm c}N_{\rm d}(r)}, \tag{11}$$

$$\dot{r}^2=E-\frac{L^2}{r^2}N_{\rm d}(r). \tag{12}$$

Here, we take a new affine parameter $\xi\to\xi/|L|$. It is worth mentioning that the impact parameter $b_{\rm c}=L/E$ (the ratio of angular momentum to energy) is introduced, whereby we can succinctly describe the trajectory behavior of light. Using Eqs. (10) and (11), we can get the other form of Eq. (12), that is

$$\dot{r}^2+V_{\rm eff}=\frac{1}{b_{\rm c}^2}, \tag{13}$$

$$V_{\rm eff}=\frac{1}{r^2}N_{\rm d}(r). \tag{14}$$

Here, $V_{\rm eff}$ is the effective potential of black hole, which is an important physical quantity to judge the deflection behavior of light around a black hole. Note that the critical one separating captured and uncaptured photons is given by the solution of the system $\dot{r}^2=0$ and $\partial_r\dot{r}^2=0$, which means

$$V_{\rm eff}=\frac{1}{b_{\rm c}^2},\quad V'_{\rm eff}=0. \tag{15}$$

Naturally, the position of the photon ring can be obtained by Eq. (15), and the radius of the photon sphere $r_{\rm p}$ and impact parameter $b_{\rm p}$ satisfy

$$r_{\rm p}^2=b_{\rm p}^2N_{\rm d}(r),\quad 2b_{\rm p}^2N_{\rm d}(r)^2=r^3N'_{\rm d}(r). \tag{16}$$

Supported by Eq. (16), we can obtain the radius $r_{\rm p}$, and impact parameter $b_{\rm p}$ of photon sphere under the different value of the geometric parameters $\kappa\lambda$ and state parameter $N_{\rm d}$ of the Rastall theory. For the different value of the parameters $\kappa\lambda$ where the values of $N_{\rm d}$ is fixed, the numerical results of radius $r_{\rm p}$ and impact parameter $b_{\rm p}$ of the photon sphere, as well as the event horizon $r_{\rm e}$ are listed in the Tables 1 and 2. For the case of parameters $\kappa\lambda$ is fixed and the value of $N_{\rm d}$ is variable, they are shown in Tables 3 and 4.

When $N_{\rm d}$ is a fixed positive value, one can see that the values of the radius $r_{\rm p}$ and impact parameter $b_{\rm p}$ of photon sphere increases with the increase of $\kappa\lambda$, as well as the event horizon $r_{\rm e}$. But in the case of $N_{\rm d}$ is a fixed negative value, the three physical quantities $r_{\rm p}$, $b_{\rm p}$ and $r_{\rm e}$ are all smaller and smaller when the value of parameters $\kappa\lambda$ is increase. For the case of $\kappa\lambda$ is fixed, $r_{\rm p}$, $b_{\rm p}$ and $r_{\rm e}$ are also show an increasing trend with the positive growth of $N_{\rm d}$, while decrease with the negative growth of $N_{\rm d}$. That is, the black hole spacetime will expand with the increase of geometric parameters $\kappa\lambda$ when the state

parameter N_d is positive, and the state parameter N_d is negative has the opposite effect. It is worth noting that the change trend of relevant physical quantities is very weak when N_d is negative. We plot the effective potential V_{eff} corresponding to the impact parameter b_c with the given value of geometric parameters $\kappa\lambda$ and state parameter N_d, as depicted in Fig. 1.

Table 1. The radius r_p, impact parameter b_p of the photon sphere and the event horizon r_e for different geometric parameters $\kappa\lambda$ when $N_d = 0.05$, in which, we take $M = 1$.

	$\kappa\lambda = 0.01$	$\kappa\lambda = 1/12$	$\kappa\lambda = 0.1$	$\kappa\lambda = 1/8$	$\kappa\lambda = 0.2$	$\kappa\lambda = 2/9$	$\kappa\lambda = 0.24$
r_e	2.05112	2.06366	2.06827	2.07754	2.15857	2.25403	2.5616
r_p	3.07685	3.09718	3.10446	3.11872	3.21631	3.2668	3.31602
b_p	5.23065	5.38563	5.4075	5.45394	5.98805	6.8956	12.6483

Table 2. The radius r_p, impact parameter b_p of the photon sphere and the event horizon r_e for different geometric parameters $\kappa\lambda$ when $N_d = -0.05$, in which, we take $M = 1$.

	$\kappa\lambda = 0.35$	$\kappa\lambda = 0.4$	$\kappa\lambda = 0.5$	$\kappa\lambda = 0.6$	$\kappa\lambda = 0.75$	$\kappa\lambda = 0.8$	$\kappa\lambda = 1$
r_e	1.99982	1.99922	1.99369	1.98936	1.98545	1.98456	1.98208
r_p	2.99996	2.99969	2.99441	2.98883	2.98322	2.98189	2.97811
b_p	5.19614	5.19597	5.19132	5.18511	5.17802	5.17623	5.17092

Table 3. The radius r_p, impact parameter b_p of the photon sphere and the event horizon r_e for different state parameter N_d when $\kappa\lambda = 1/5$, in which, we take $M = 1$.

	$N_d = 0.01$	$N_d = 0.02$	$N_d = 0.05$	$N_d = 0.08$	$N_d = 0.1$	$N_d = 0.12$	$N_d = 0.18$
r_e	2.0289	2.05909	2.15857	2.2744	2.36331	2.46419	2.87955
r_p	3.03975	3.08113	3.21631	3.37143	3.48872	3.61983	4.13523
b_p	5.33522	5.48298	5.98805	6.61334	7.12217	7.73197	10.6659

Table 4. The radius r_p, impact parameter b_p of the photon sphere and the event horizon r_e for different state parameter N_d when $\kappa\lambda = 1/2$, in which, we take $M = 1$.

	$N_d = -0.01$	$N_d = -0.02$	$N_d = -0.05$	$N_d = -0.08$	$N_d = -0.1$	$N_d = -0.12$	$N_d = -0.18$
r_e	1.99875	1.99749	1.99369	1.98985	1.98726	1.98465	1.97669
r_p	2.99889	2.99777	2.99441	2.99103	2.98876	2.98648	2.97959
b_p	5.19519	5.19422	5.19132	5.1884	5.18645	5.18449	5.17856

In Fig. 1, we take $\kappa\lambda = 0.2$ and $N_d = 0.05$ as an example. It shows the interior of the event horizon of black hole, namely, $(r < r_b)$, and there is no effective potential V_{eff}. However, the effective potential increases from the horizon and reaches its maximum at the position of photon sphere, and after that, there is a decreasing trend. Therefore, there are several different situations when a light ray moves in the radially inward direction. As the special case of $b_c = b_p$, the light ray is in a critical state of being captured and escaping, and it will rotate around the black hole infinitely many times due to the angular velocity is not zero. This is corresponding to the region 2 (red lines) in Fig. 1. If the light ray motion at the region 1 ($b_c > b_p$) in Fig. 1, the light will encounter the potential barrier and then be reflected back in the outward direction, that is, the photons in this region do not fall into the black hole and can reach the observer at infinity. When the light ray motion at region 3 ($b_c < b_p$) in Fig. 1, which leads to the light ray through the event horizon and go straight into the black hole and the observer will not capture the light in this region. In order to explore the change of effective potential V_{eff} when the relevant parameters change, the effective potential V_{eff} of black hole under the different value of $\kappa\lambda$ and N_d is shown in Fig. 2.

From Fig. 2(a), one can find that the peak value of the effective potential V_{eff} increases with the decrease of $\kappa\lambda$ when the value of N_d is fixed ($N_d > 0$), and changes obviously. While the negative N_d ($N_d < 0$) has the opposite effect, i.e., the peak value of the effective potential V_{eff} increases with the increase of $\kappa\lambda$, but the degree of change is so weak that it can hardly be distinguished, as shown in Fig. 2(b). In Figs. 2(c) and 2(d), the value of $\kappa\lambda$ is fixed. The peak value of the effective potential V_{eff} also decreases with the positive increase of N_d and the trend of change is also obvious. However, the peak value of the effective potential V_{eff} increases with the negative growth of N_d when $\kappa\lambda$ is fixed, but the trend of change is very weak.

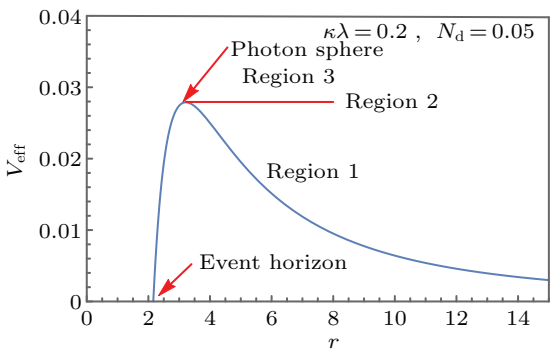


Fig. 1. The profiles of the effective potential V_{eff} as a function of impact parameter b_c, in which $\kappa\lambda = 0.2$ and $N_d = 0.05$. Here, we take $M = 1$.

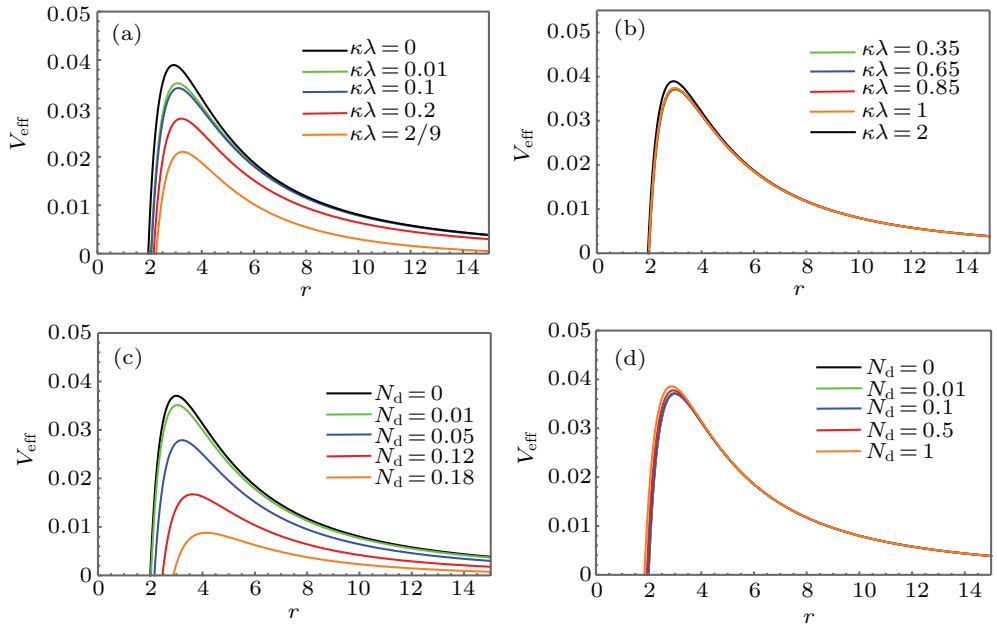


Fig. 2. The profiles of the effective potential $V_{\rm eff}$ as a function of impact parameter $b_{\rm c}$ for the different value of $\kappa\lambda$ and $N_{\rm d}$. (a) and (b) The value of $\kappa\lambda$ is various and the value of $N_{\rm d}$ is fixed ($N_{\rm d} = 0.05$ and $N_{\rm d} = -0.05$). (c) and (d) The value of $N_{\rm d}$ is various and the value of $\kappa\lambda$ is fixed ($\kappa\lambda = 0.2$ and $\kappa\lambda = 0.5$). Here, we take $M = 1$.

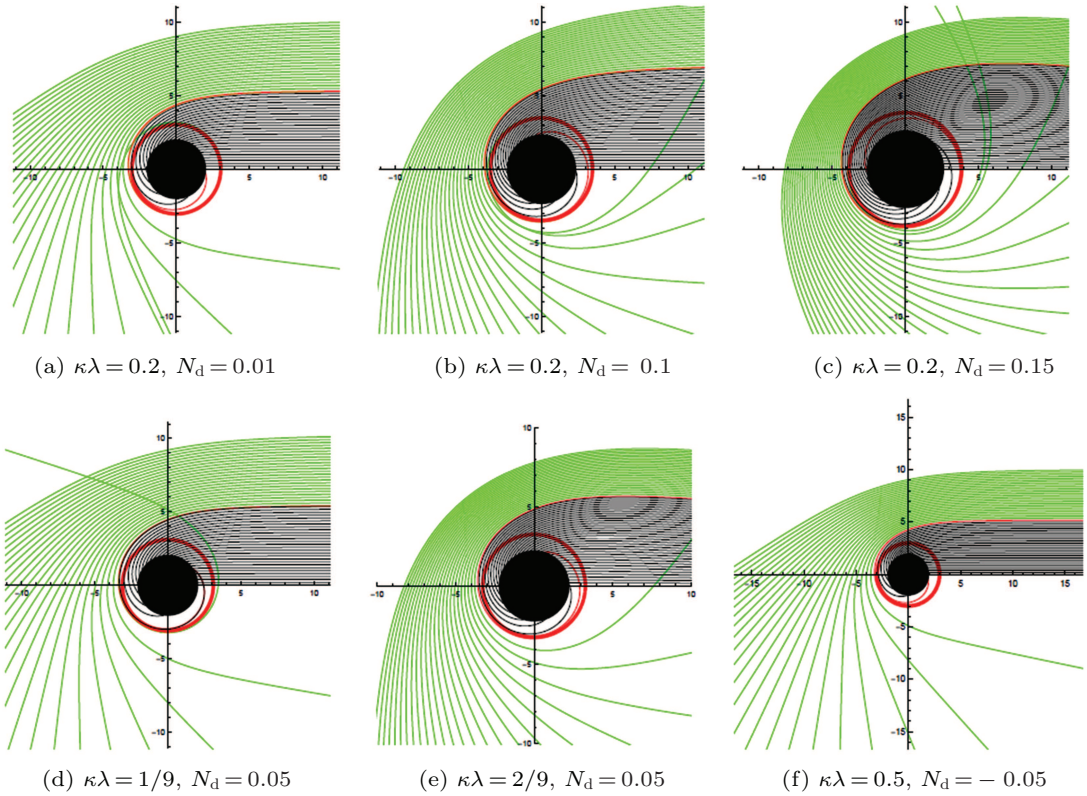


Fig. 3. The trajectory of the light ray for the different value of $\kappa\lambda$ and $N_{\rm d}$ in the polar coordinates (r, φ), in which, the region of black hole is shown as a solid disk and the position of photon sphere as a dashed red line.

With the help of Eqs. (10) and (11), we can get the concrete expression of photon motion equation, which is

$$\frac{{\rm d}r}{{\rm d}\varphi} = \pm r^2 \sqrt{\frac{1}{b^2} - \frac{1}{r^2}\left[1 - \frac{2M}{r} - \frac{N_{\rm d}}{r^{\frac{1-6\kappa\lambda}{1-3\kappa\lambda}}}\right]}. \tag{17}$$

Here, we introduce a parameter $u = 1/r$, and Eq. (17) can be rewritten as

$$\mathcal{R}(u,b) \equiv \frac{{\rm d}u}{{\rm d}\varphi} = \sqrt{\frac{1}{b^2} - u^2\left[1 - 2Mu - N_{\rm d}\left(\frac{1}{u}\right)^{-\frac{1-6\kappa\lambda}{1-3\kappa\lambda}}\right]}. \tag{18}$$

Using the ray-tracing code,[42] we can plot the trajectory of the light ray for the different state parameters $\kappa\lambda$ and $N_{\rm d}$, which are shown in Fig. 3.

In the case of $b_c > b_p$ (green lines), the trajectory of the light ray deflects, i.e., the light ray move toward the black hole from infinity approaching one closest point and then move away from the black hole back to infinity. In the case of $b_c < b_p$ (black lines), one can find that all the light ray falls into the black hole and cannot return to the observer's position. In particular, $b_c = b_p$, which corresponds to the area of red dotted line, the light ray just revolve around the black hole, neither entering nor escaping from it, i.e., the position of photon sphere. The key problem is to find the turning point where the light deflects owing to the light changing its radial direction, and the turning point corresponds to the minimally positive real root of Eq. (18). In Fig. 3, we can see that the trajectory and deflection of light near the black hole change with the different value of geometric parameters $\kappa\lambda$ and state parameter N_d in the spacetime Eq. (2). In other words, the light density that can be obtained by observers at infinity is different, which will naturally lead to the different observation appearance of black holes.

3. The shadows and photon spheres in different spherical accretions scenarios

With the previous preparations, we intend to further investigate the observed property and intensity of black hole shadow in the spacetime Eq. (2). In this section, we consider that thin spherical accretion is covered on a gravitating object, and two different models are given, i.e., the static spherical accretion and infalling spherical accretion.

3.1. The static spherical accretion

For the static spherical accretion model, it is considered that the accretion material is in a resting state, and the radiation of the material is isotropic. Hence, the intensity of radiation I_{obs} (erg $\cdot$ s^{-1} $\cdot$ cm^{-2} $\cdot$ str^{-1} $\cdot$ Hz^{-1}) with the observed photon frequency ν_{obs} for the distant observer ($r_o \to \infty$) can be taken as[76,77]

$$I_{obs}(\nu_{obs}) = \int_\gamma g^3 j(\nu_e)\, dl_{prop}, \tag{19}$$

with

$$g = \nu_o/\nu_e. \tag{20}$$

Here, g, ν_e and ν_o are the redshift factor, emitter photon frequency and observed photon frequency, respectively. In the rest frame of the emitter, $j(\nu_e)$ is the emissivity per unit volume, and dl_{prop} is the infinitesimal proper length which is differential as measured in the frame comoving with the matter. In the spacetime Eq. (2), the redshift factor is

$$g = N_d(r)^{1/2}. \tag{21}$$

Considering a simple model that the radiation of light is monochromatic with a fixed frequency ν_f, we can get

$$j(\nu_e) \propto \frac{\delta(\nu_e - \nu_f)}{r^2}, \tag{22}$$

$$dl_{prop} = \sqrt{\frac{1}{N_d(r)}dr^2 + r^2 d\varphi^2}. \tag{23}$$

Note that Eq. (22) takes the radial profile as $1/r^2$, and δ is the delta function. Then, we can rewrite Eq. (23) as

$$dl_{prop} = \sqrt{\frac{1}{N_d(r)} + r^2\left(\frac{d\varphi}{dr}\right)^2}\, dr. \tag{24}$$

On the basis of Eq. (17), the specific intensity $I_{obs}(\nu_{obs})$ observed by a distance observer is

$$I_{obs}(\nu_{obs}) = \int_\gamma \frac{N_d(r)^{3/2}}{r^2}\sqrt{\frac{1}{N_d(r)} + r^2\left(\frac{d\varphi}{dr}\right)^2}\, dr. \tag{25}$$

From Eq. (25), one can find that the observed luminosity of black hole shadow largely depends on the state parameters of the spacetime Eq. (2), as well as the impact parameter b_c. It is worth mentioning that the intensity is circularly symmetric with the impact parameter b_c of the radius, which satisfies $b^2 = x^2 + y^2$. Therefore, turn our attention to research the change of intensity $I_{obs}(\nu_{obs})$ with the impact parameter b_c when $\kappa\lambda$ and N_d are taken as different values. In Fig. 4, we show the specific intensity $I_{obs}(\nu_{obs})$ as a function of impact parameter b_c for the different parameters $\kappa\lambda$ and N_d.

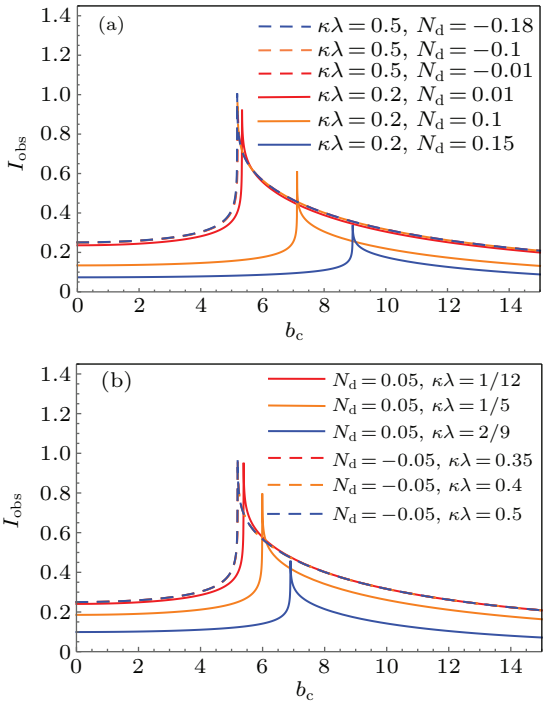


Fig. 4. Profiles of the specific intensity I_{bos} seen by a distant observer for the static spherical accretion. (a) The value of N_d is various and $\kappa\lambda$ is fixed ($\kappa\lambda = 0.2$ and $\kappa\lambda = 0.5$). (b) The value of $\kappa\lambda$ is various and N_d is fixed ($N_d = 0.05$ and $N_d = -0.05$). Here, we take $M = 1$.

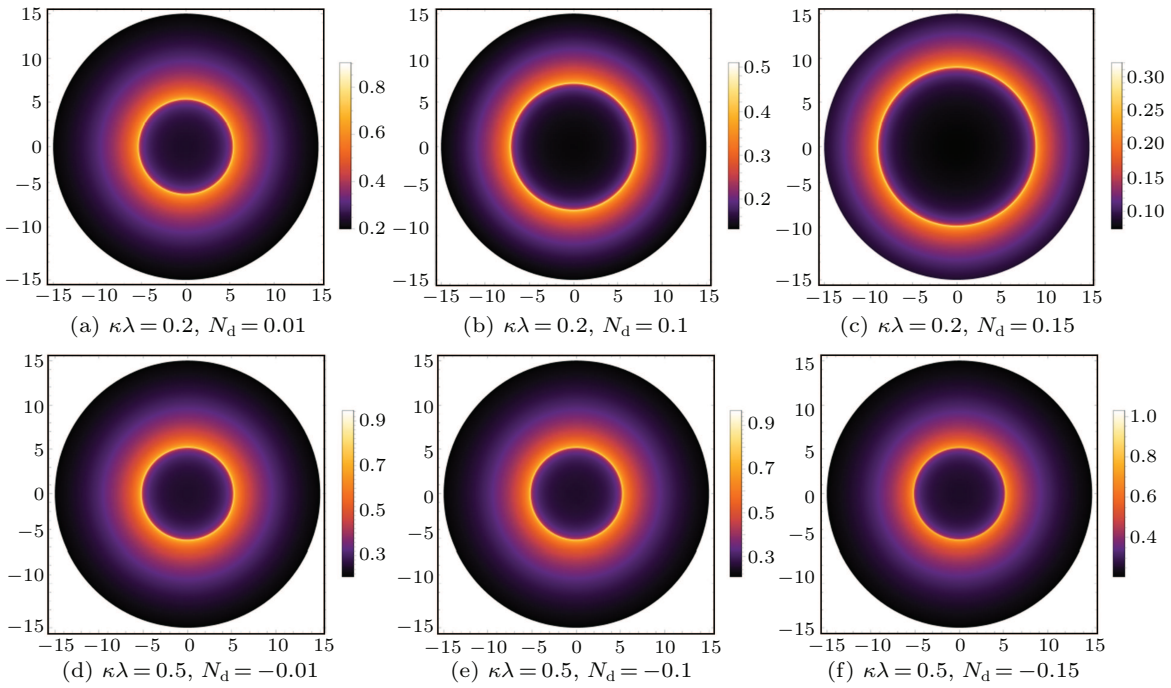


Fig. 5. Profiles of the specific intensity $I_{\rm obs}$ seen by a distant observer for a static spherical accretion under the different relevant parameters ($\kappa\lambda$ and $N_{\rm d}$).

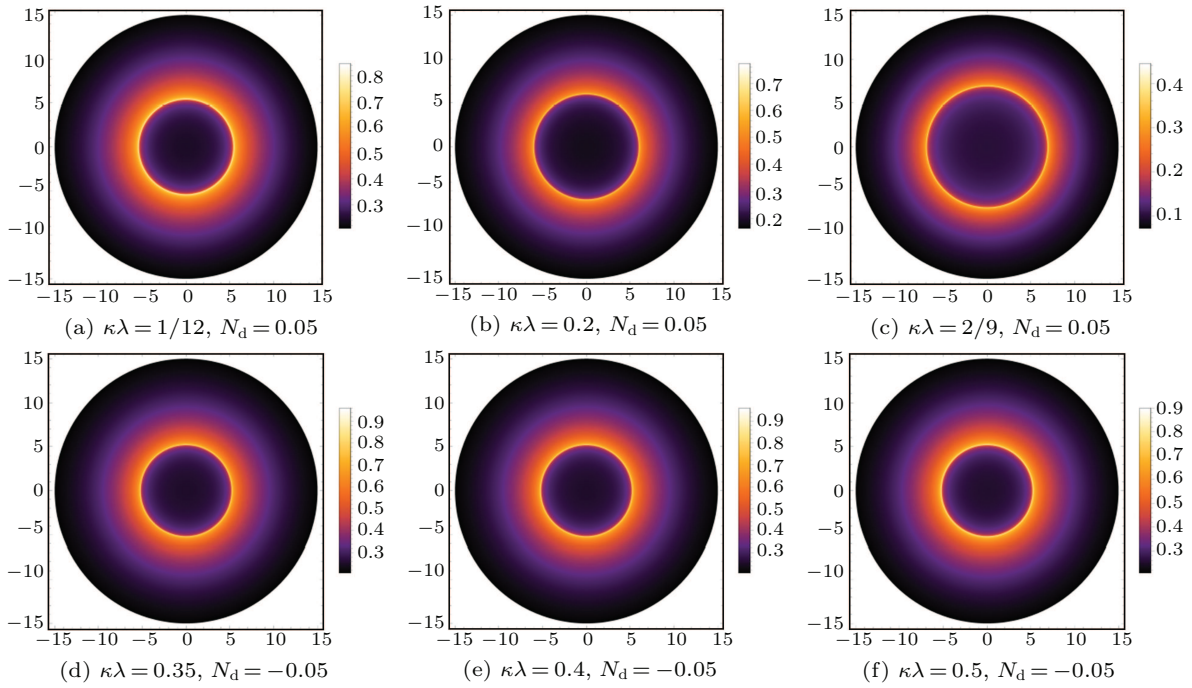


Fig. 6. Profiles of the specific intensity $I_{\rm obs}$ seen by a distant observer for a static spherical accretion under the different relevant parameters ($\kappa\lambda$ and $N_{\rm d}$).

Obviously, although the parameters $\kappa\lambda$ and $N_{\rm d}$ are taken as different values, the observed intensity $I_{\rm obs}(\nu_{\rm obs})$ always reaches the peak at the position of $b_{\rm c} = b_{\rm p}$. Since the light ray revolves around the black hole many times and collects an arbitrarily large intensity, the intensity increases sharply and reaches the peak value. For the case of $b_{\rm c} > b_{\rm p}$, the intensity of observer is mainly contributed by the refracted light, so that the intensity decreases with the increase of $b_{\rm c}$. If the value of $b_{\rm c}$ is large enough, the refracted light tends to disappear, which thus leads to the vanishing of observed intensity. Due to the intensity originating from the accretion is absorbed mostly by the black hole in the case of $b_{\rm c} < b_{\rm p}$, the observers rarely capture intensity. However, there is a part of the radiation escaped from the black hole. Hence, the specific intensity does not disappear completely with a small finite value.

Furthermore, the different parameters of $\kappa\lambda$ and $N_{\rm d}$ will cause the observer to obtain different observation intensities $I_{\rm obs}(\nu_{\rm obs})$. When the parameters $\kappa\lambda$ are given, the observation

intensity will decrease with the positive growth of parameter $N_{\rm d}$, and the degree of weakening is very obvious. While the observation intensity will increase with the negative growth of parameter $N_{\rm d}$, but its growth degree is very small, which leads that we can not clearly distinguish the dotted line in Fig. 4(a). When the parameter $N_{\rm d}$ is fixed as a positive value, the increase of parameter $\kappa\lambda$ will also significantly weaken the observation intensity. In the case of $N_{\rm d}$ taken as a negative value, the increase of parameter $\kappa\lambda$ promotes the observation intensity, but the increase degree is so small that the dotted lines is shown almost superposed in Fig. 4(b). In order to make our result more visible, we show the shadow images and the corresponding intensities as seen by a distant observer for the different values of parameters $\kappa\lambda$ and $N_{\rm d}$, and shown in Figs. 5 and 6.

From the top row of Fig. 5, one can see that for a given value of parameters $\kappa\lambda$ ($\kappa\lambda = 0.2$), the shadow size increases with the larger value of $N_{\rm d}$, but the observed intensity decreases. In the bottom row of Fig. 5, the parameters $\kappa\lambda = 0.5$ and $N_{\rm d}$ show a negative growth trend, and not only the change of the observed intensity is very weak, but also the radius of the shadow has small change. As shown in the top row of Fig. 6, the observed intensity has been weaken with the positive increase of parameters $\kappa\lambda$, but the shadow radius of the black hole shows the opposite trend. In the bottom row of Fig. 6, the change of both shadow radius and observed intensity are weak with the change of $\kappa\lambda$, where the parameter $N_{\rm d}$ is fixed as a negative value. And the impact of change of $\kappa\lambda$ is almost nil. Hence, the state parameters $\kappa\lambda$ and $N_{\rm d}$ play an important role for the observed intensity, and the change of those values will directly affect the observed intensity of the distant observer.

3.2. The infalling spherical accretion

In this section, we start with a more realistic model, i.e., the optically thin accretion moves towards the black hole, due to the most accretion matters in the universe should not be static. Here, the optically thin accretion is considered to be infalling matters, which is a real accretion flow process. For simplicity, we also take the radiation power and emission coefficient, as measured in the rest frame of the infalling accretion. Along the way, the velocity of the infalling accretion will affect the redshift factor of accretion. And the redshift factor of infalling accretion can be expressed as[47]

$$g_i = \frac{k_\alpha u^\alpha_{\rm obs}}{k_\beta u^\beta_{\rm e}}, \tag{26}$$

where $k^\mu = \dot{x}_\mu$ is the four-velocity of the photon. In addition, $u^\mu_{\rm e}$ is the four-velocity of the accreting matter emitting the radiation, and $u^\mu_{\rm obs} = (1,0,0,0)$ is the four-velocity of the distant observer. We assume that the accretion matter in radial is free and falls with the four-velocity, which in the spherically symmetric case of spacetime Eq. (2) reduces to

$$u^t_{\rm e} = \frac{1}{N_{\rm d}(r)}, \quad u^r_{\rm e} = -\sqrt{1 - N_{\rm d}(r)}, \quad u^\theta_{\rm e} = u^\phi_{\rm e} = 0. \tag{27}$$

For the photons, the four-velocity was found in Eqs. (10)–(12). With the constant of $k_t = 1/b_{\rm c}$ and $k_\gamma k^\gamma = 0$, we can get k_γ as

$$\frac{k_\gamma}{k_t} = \pm\frac{1}{N_{\rm d}(r)}\sqrt{N_{\rm d}(r)\left(\frac{1}{N_{\rm d}(r)} - \frac{b_{\rm c}^2}{r^2}\right)}, \tag{28}$$

where the sign $+$ $(-)$ indicates that the photon approaches (goes) away from the black hole. The redshift factor in Eq. (26) is given by

$$g_i = \frac{1}{u^t_{\rm e} + k_\gamma/k_{\rm e} u^r_{\rm e}}. \tag{29}$$

Then, the proper length $\mathrm{d}l_{\rm prop}$ can be written as

$$\mathrm{d}l_{\rm prop} = k_\gamma u^\gamma_{\rm e}\mathrm{d}\xi = \frac{k_t}{g_i\,|k_r|}\mathrm{d}r, \tag{30}$$

in which, ξ is the affine parameter along the photon path γ, and λ has to be evaluated along the path of the photon. Integrating the intensity over all the observed frequencies, we obtain the observed flux, that is

$$I_{\rm f(obs)}(\nu_{\rm obs}) \propto \int_{\gamma_i} \frac{g_i^3 k_t}{r^2\,|k_r|}\mathrm{d}r. \tag{31}$$

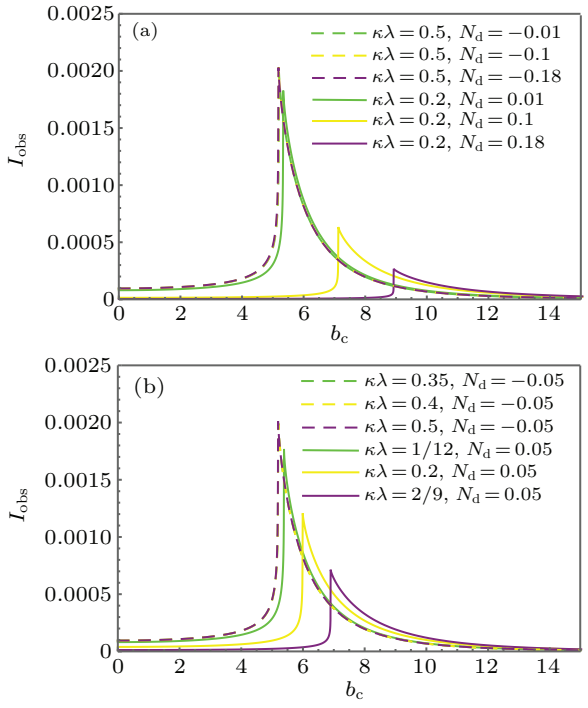


Fig. 7. Profiles of the specific intensity $I_{\rm obs}$ seen by a distant observer for the infalling spherical accretion. (a) The value of $N_{\rm d}$ is various and $\kappa\lambda$ is fixed ($\kappa\lambda = 0.2$ and $\kappa\lambda = 0.5$). (b) The value of $\kappa\lambda$ is various and $N_{\rm d}$ is fixed ($N_{\rm d} = 0.05$ and $N_{\rm d} = -0.05$). Here, we take $M = 1$.

Now, we still take different value of geometric parameters $\kappa\lambda$ and state parameters $N_{\rm d}$ for investigating the shadow of the black hole with an infalling accretion, as shown in Fig. 7. From Fig. 7, the peak value of luminosity is much lower than

that of static accretion model, which is the most significant difference for both the static and infalling accretion models. Moreover, there is a sharp rise before the luminosity reaching its peak for the infalling spherical accretion models, i.e., the change rate of intensity of the infalling accretion is greater than that of static accretion. It shows that the absorption rate of photons by black holes is higher than the static case. When the value of parameters $\kappa\lambda$ increase and $N_{\rm d}$ is fixed as a positive value (or $\kappa\lambda$ is fixed and $N_{\rm d}$ is positive growth), the peak values of luminosity showed an obvious downward trend. While for the parameter $N_{\rm d}$ is negative value and parameters $\kappa\lambda$ increase (or $\kappa\lambda$ is fixed and $N_{\rm d}$ is negative growth), the peak values of luminosity will increases but the change is very small.

In addition, the corresponding two dimensional images of the intensity are drawn in Figs. 8 and 9. Comparing with the static case, the central region for the infalling case is darker, and the light intensity that the observer can obtain is much smaller. This is caused by the Doppler effect here. However, the radius of the shadow and the position of the photon sphere are consistent under the different accretion (the static and

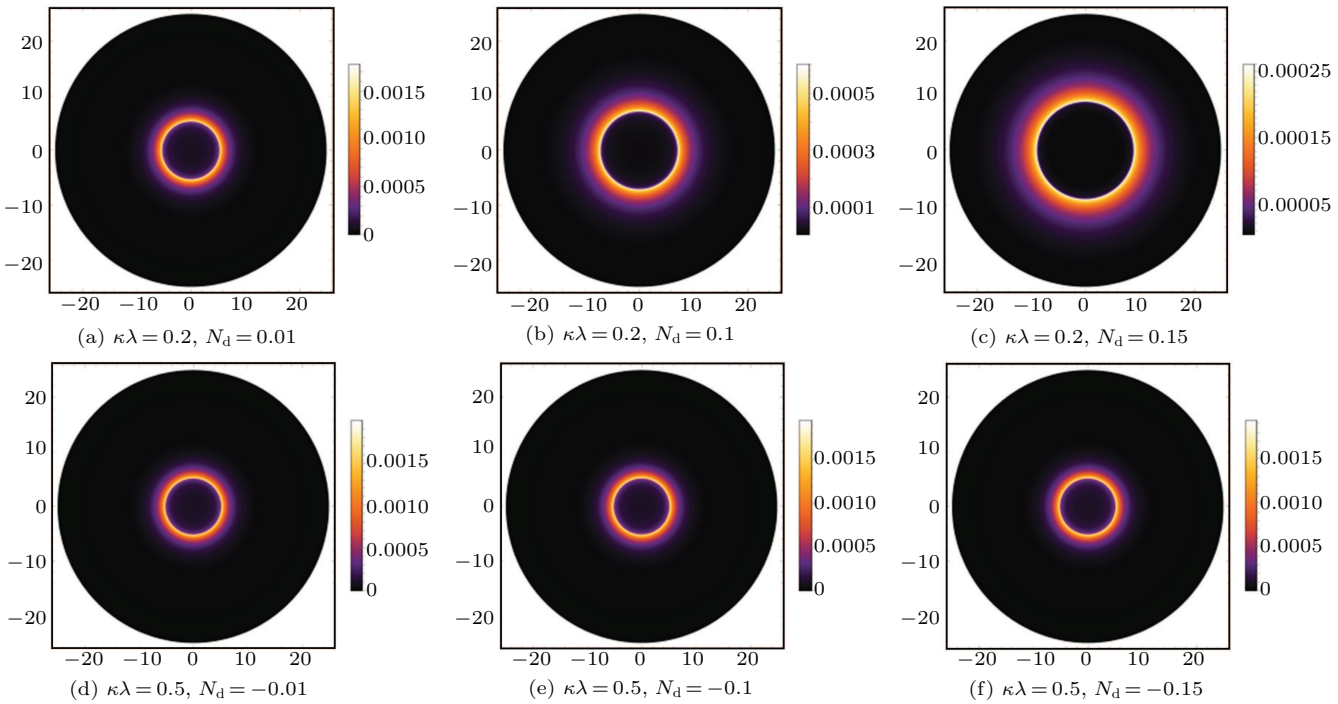


Fig. 8. Profiles of the specific intensity $I_{\rm obs}$ seen by a distant observer for a static spherical accretion under the different relevant parameters ($\kappa\lambda$ and $N_{\rm d}$).

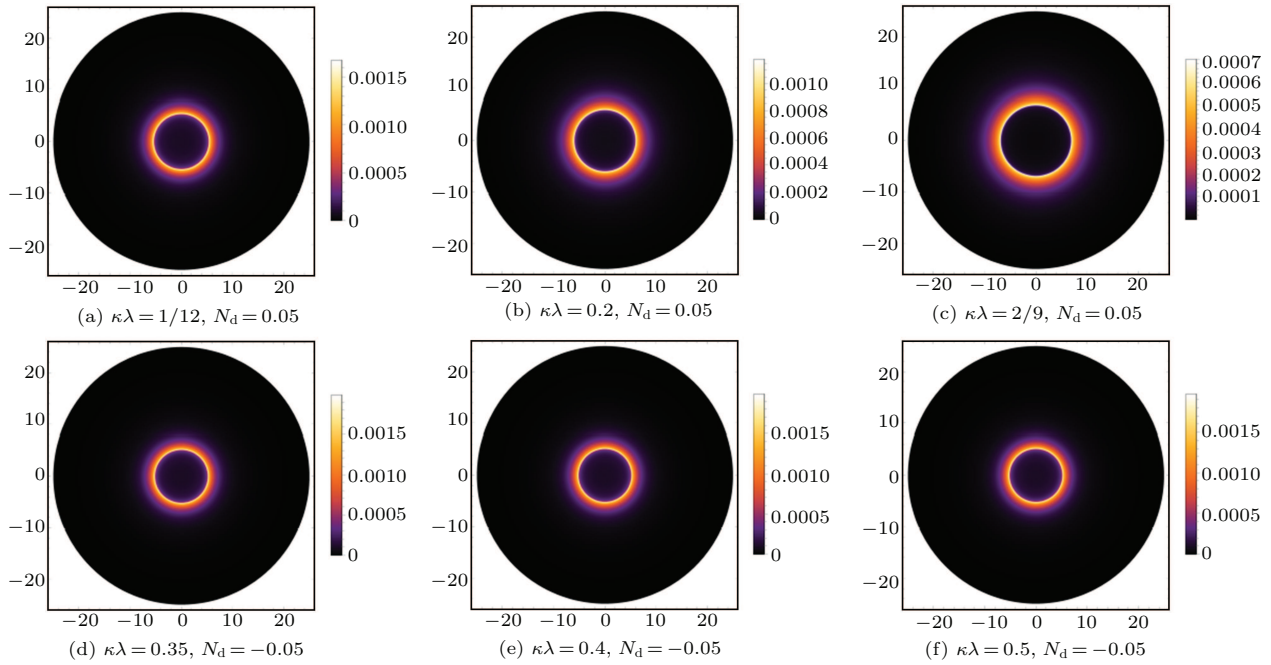


Fig. 9. Profiles of the specific intensity $I_{\rm obs}$ seen by a distant observer for a static spherical accretion under the different relevant parameters ($\kappa\lambda$ and $N_{\rm d}$).

infalling spherical accretion), which means that the different accretion model affect the observable intensity of shadows but does not affect the geometry structure of spacetime.

4. Discussion and conclusion

In the scenario of Rastall gravity theory, the shadow and observation appearance of black hole immersed in dust field have been studied in detail. It is shown that the radius of event horizon r_e, photon sphere r_e, and critical impact parameter b_p of the black hole have interesting characteristics depending on the different ranges of the parameters in Rastall theory. Specifically, these three related physical quantities all show a significant increase as the increase of Rastall geometric parameters $\kappa\lambda$, where the field structure parameter N_d is given, as well as the case of N_d increases where the value of $\kappa\lambda$ is fixed. But if the parameters $\kappa\lambda$ increase and N_d is a fixed negative value, or the parameters $\kappa\lambda$ are fixed and N_d is negative growth, both the physical quantities r_e, r_p and b_p will show weak decreasing trend. Naturally, the increase of $\kappa\lambda$ (N_d is fixed as a positive value) or the positive growth of N_d ($\kappa\lambda$ is fixed) will significantly reduce the peak value of effective potential. While the parameter N_d is negative (or is negative growth), it has a positive effect on the effective potential.

When the values of Rastall geometric parameters $\kappa\lambda$ and state parameter N_d change, it can be found that not only the shadow radius of the black hole changes, but also the deflection degree of light ray near the black hole changes. Therefore, the light density that can be obtained by an observer at infinity is different, which will naturally lead to the different observation appearance and intensity of the black hole shadow. In order to intuitively reflect the change of shadow observation characteristics caused by the change of relevant parameters ($\kappa\lambda$ and N_d), we calculate the specific intensity observed by an infinite observer, and also give the profile image of black hole shadow in different relevant parameters. In system (7), we consider that the accretion radiation is the only background light source, and mainly take two accretion models, i.e., the static and infalling spherical accretions, which are optically and geometrically thin.

For the case of static spherically accretions, the inner region of the black hole shadow is not completely dark, and the peak of observed intensity is always near the position of the photon sphere. One can find that the peak of observed intensity is attenuated with the increase of parameters $\kappa\lambda$ in the case of parameter N_d is fixed as a positive value, while is enhancement with the increase of parameters $\kappa\lambda$ in the case of parameter N_d is fixed as a negative value. When parameter $\kappa\lambda$ is taken as a fixed value, the peak value of observation intensity will decrease with the positive growth of parameter N_d, but increase with the negative growth of N_d. For the case of infalling spherical accretion, the change trend of observation intensity caused by the change of relevant parameters is similar to that of static model, but the change degree is greater than that of static model. Meanwhile, both the inner region and the outer observable bright region of the black hole shadow are obviously darker than the static accretion model. And the peak value of the observed intensity is about two orders of magnitude lower than that of the static model. Doppler effect is the reason for the significant difference of observation intensity between these two different accretion modes. For different spherical accretions background, the weakening of observation intensity caused with the variation with parameters ($\kappa\lambda$ and N_d) is very obvious, but the degree of enhancement is very weak. As shown in Fig. 4 for the static model (Fig. 7 for the infalling model), the dotted lines almost coincide and the change of peak value is very weak, which can also be reflected from the bottom row of Figs. 5 and 6 (Figs. 8 and 9 for the infalling model). The increase extent of observation intensity is very weak and can even be ignored. Moreover, the size and position of black hole shadow do not change in the both case of accretion models. It is implied that the black hole shadow is caused by spacetime geometry, which is determined by the geometric parameters $\kappa\lambda$ and state parameter N_d in the background of Rastall gravity theory. Put forward, it could be a feasible method to explore the structural parameters of spacetime from the observation of black hole shadow.

Acknowledgements

Project supported by the National Natural Science Foundation of China (Grant Nos. 11875095 and 11903025) and Basic Research Project of Science and Technology Committee of Chongqing (Grant No. cstc2018jcyjA2480).

References

[1] Abbott B P, *et al*. 2016 *Phys. Rev. Lett.* **116** 241103
[2] Abbott B P, *et al*. 2016 *Phys. Rev. Lett.* **116** 241102
[3] Abbott B P, *et al*. 2016 *Phys. Rev. Lett.* **116** 061102
[4] Akiyama K, *et al*. 2019 *Astrophys. J.* 875 L1
[5] Akiyama K, *et al*. 2019 *Astrophys. J. Lett.* 875 L4
[6] Akiyama K, *et al*. 2019 *Astrophys. J. Lett.* 875 L5
[7] Akiyama K, *et al*. 2019 *Astrophys. J. Lett.* 875 L6
[8] Synge J L 1966 *Mon. Not. Roy. Astron. Soc.* **131** 463
[9] Luminet J P 1979 *Astron. Astrophys.* **75** 228
[10] Bardeen J M 1972 *Timelike and null geodesics in the Kerr metric, in Black Holes* (Les Astres Occlus: Les Houches) pp. 215–239
[11] Chandrasekhar S 1983 *The Mathematical Theory of Black Holes* (Oxford: Oxford University Press)
[12] Falcke H, Melia F and Agol E 2000 *Astrophys. J.* **528** L13
[13] Shaikh R, Kocherlakota P, Narayan R and Joshi P S 2019 *Mon. Not. Roy. Astron. Soc.* **482** 52
[14] Banerjee I, Chakraborty S and SenGupta S 2020 *Phys. Rev. D* **101** 041301
[15] Vagnozzi S and Visinelli L 2019 *Phys. Rev. D* **100** 024020
[16] Vagnozzi S, Bambi C and Visinelli L 2020 *Class. Quant. Grav.* **37** 087001
[17] Safarzadeh M, Loeb A and Reid M 2019 *Mon. Not. Roy. Astron. Soc.* **488** L90
[18] Davoudiasl H and Denton P B 2019 *Phys. Rev. Lett.* **123** 021102
[19] Roy R and Yajnik U A 2020 *Phys. Lett. B* **803** 135284

[20] Chen Y F, Shu J, Xue X, Yuan Q and Zhao Y 2020 *Phys. Rev. Lett.* **124** 061102
[21] Amarilla L, Eiroa E F and Giribet G 2010 *Phys. Rev. D* **81** 124045
[22] Li Z L and Bambi C 2014 *JCAP* **01** 041
[23] Grenzebach A, Perlick V and Lämmerzahl C 2014 *Phys. Rev. D* **89** 124004
[24] Contreras E, Rincón Á, Panotopoulos G, Bargue ño P and Koch B 2020 *Phys. Rev. D* **101** 064053
[25] Wei S W and Liu Y X 2021 *Eur. Phys. J. Plus* **136** 436
[26] Hu Z Z, Zhong Z, Li P C, Guo M Y and Chen B 2021 *Phys. Rev. D* **103** 044057
[27] Guo M Y and Li P C 2020 *Eur. Phys. J. C* **80** 588
[28] Chang Z and Zhu Q H 2020 *Phys. Rev. D* **102** 044012
[29] Guo Y and Miao Y G 2020 *Phys. Rev. D* **102** 084057
[30] Long F, Wang J C, Chen S B and Jing J L 2019 *JHEP* **10** 269
[31] Guo H, Liu H, Kuang X M and Wang B 2020 *Phys. Rev. D* **102** 124019
[32] Wei S W and Liu Y X 2013 *JCAP* **11** 063
[33] Wei S W, Cheng P, Zhong Y and Zhou X N 2015 *JCAP* **08** 004
[34] Huang Y, Chen S B and Jing J L 2016 *Eur. Phys. J. C* **76** 594
[35] Wang H M, Xu Y M and Wei S W 2019 *JCAP* **03** 046
[36] Neves J C S 2020 *Eur. Phys. J. C* **80** 717
[37] Chen D Y, Gao C H, Liu X M and Yu C Y 2021 *Eur. Phys. J. C* **81** 700
[38] Çimdiker İ, Demir D and Övgün A 2021 *Phys. Dark Univ.* **34** 100900
[39] Javed W, Hamza A and Övgün A 2021 *Universe* **7** 385
[40] Okyay M and Övgün A 2022 *JCAP* **01** 009
[41] Porth O, *et al*. 2019 *Astrophys. J. Suppl.* **243** 26
[42] Narayan R, Johnson M D and Gammie C F 2019 *Astrophys. J.* **885** L33
[43] Cunha P V P, Eiró N A, Herdeiro C A R and Lemos J P S 2020 *JCAP* **2003** 035
[44] Zeng X X, Zhang H Q and Zhang H B 2020 *Eur. Phys. J. C* **80** 872
[45] Qin X, Chen S B and Jing J L 2021 *Class. Quant. Grav.* **38** 115008
[46] Gralla S E, Holz D R and Wald R M 2019 *Phys. Rev. D* **100** 024018
[47] Zeng X X and Zhang H Q 2020 *Eur. Phys. J. C* **80** 1058
[48] Gan Q Y, Wang P, Wu H W and Yang H T 2021 *Phys. Rev. D* **104** 024003
[49] Peng J, Guo M Y and Feng X H 2021 *Chin. Phys. C* **45** 085103
[50] He K J, Tan S C and Li G P 2022 *Eur. Phys. J. C* **82** 81
[51] Li G P and He K J 2021 *Eur. Phys. J. C* **81** 1018
[52] Zeng X X, He K J and Li G P 2022 *Sci. China Phys. Mech. Astron.* **65** 290411
[53] Zeng X X, Li G P and He K J 2022 *Nucl. Phys. B* **974** 115639
[54] Li G P and He K J 2021 *JCAP* **06** 037
[55] Peng J, Guo M Y and Feng X H 2021 *Phys. Rev. D* **104** 124010
[56] Gralla S E and Lupsasca A 2020 *Phys. Rev. D* **101** 044031
[57] He K J, Guo S, Tan S C and Li G P 2022 *Chin. Phys. C* **46** 085106
[58] Guo S, Li G R and Liang E W 2022 *Phys. Rev. D* **105** 023024
[59] Zhu Y N and Wang T 2021 *Phys. Rev. D* **104** 104052
[60] Guerrero M, Olmo G J, Rubiera-Garcia D and Gómez D S C 2021 *JCAP* **08** 036
[61] Gan Q Y, Wang P, Wu H W and Yang H T 2021 *Phys. Rev. D* **104** 044049
[62] Hou Y H, Guo M Y and Chen B 2021 *Phys. Rev. D* **104** 024001
[63] Saurabh K and Jusufi K 2021 *Eur. Phys. J. C* **81** 490
[64] Rastall P 1972 *Phys. Rev. D* **6** 3357
[65] Rastall P 1976 *Can. J. Phys.* **54** 66
[66] Heydarzade Y and Darabi F 2017 *Phys. Lett. B* **771** 365
[67] Pourhassan B and Upadhyay S 2021 *Eur. Phys. J. Plus* **136** 311
[68] Lobo I P, Moradpour H, Morais Graça J P and Salako I G 2018 *Int. J. Mod. Phys. D* **27** 1850069
[69] Kumar R, Singh B P, Ali M S and Ghosh S G 2021 *Phys. Dark Univ.* **34** 100881
[70] Soroushfar S, Saffari R and Upadhyay S 2019 *Gen. Rel. Grav.* **51** 130
[71] Lobo I P, Richarte M G, Morais Graça J P and Moradpour H 2020 *Eur. Phys. J. Plus* **135** 550
[72] Gogoi D J and Goswami U D 2021 *Phys. Dark Univ.* **33** 100860
[73] Guo S, He K J, Li G R and Li G P 2021 *Class. Quant. Grav.* **38** 165013
[74] Kiselev V V 2003 *Class. Quant. Grav.* **20** 1187
[75] Vikman A 2005 *Phys. Rev. D* **71** 023515
[76] Jaroszynski M and Kurpiewski A 1997 *Astron. Astrophys.* **326** 419
[77] Bambi C 2013 *Phys. Rev. D* **87** 107501